Heat capacity of multilayer methane on graphite: Phase transitions in the first four layers

M. J. Lysek,* M. A. LaMadrid, P. K. Day, and D. L. Goodstein
Condensed Matter Physics 114-36, California Institute of Technology, Pasadena, California 91125
(Received 15 June 1992; revised manuscript received 21 September 1992)

We present high-resolution heat-capacity data for methane adsorbed on graphite for nominal coverages of 0.87 to 7 layers, from $T=70$ to 120 K. For films thicker than 1.1 layers, we find capillary condensate coexisting with the film. We have performed heat-capacity scans on films formed by both adsorption and desorption. By comparing the locations of the phase transitions in the chemical potential μ vs T plane, we find that there is no significant interaction between the film and the capillary condensate. The heat-capacity signals from the films map out an unexpectedly rich set of phenomena for the second, third, and fourth layers, including a two-dimensional triple point and a liquid-gas coexistence region for each layer. The fourth-layer critical temperature we find is lower than previous values found by vapor-pressure isotherms.

I. INTRODUCTION

The thermodynamics of adsorbed multilayers has been the object of intense study for the past decade but many questions are still unresolved. A recent review by Hess[1] enumerates the systems that have been studied and the points out these unresolved issues. The particular system methane on graphite has been used to study two-dimensional (2D) monolayer phase transitions, wetting and nonwetting, layering, roughening, melting, and the evolution from 2D to 3D behavior. Tools that have been used include calorimetry[2–4] and vapor-pressure isotherms,[2,5–9] neutron diffraction,[10–12] electron diffraction,[13] and nuclear magnetic resonance (NMR).[14–17] A recent review of multilayer methane films on graphite may be found in Ref. 18.

In this paper, we present heat-capacity data between 70 and 120 K, for nominal coverages of less than 1 up to 7 layers. The data were taken using a homemade scanning ratio calorimeter. The questions we tried to answer are as follows: What happens to the melting transition in the extended monolayer regime? How do the second and higher layers behave as the film grows? How do the substrate and the neighboring layers affect each layer's behavior? Can the effects of capillary condensation be distinguished from the behavior of the film?

Monolayer methane on graphite has been studied extensively up to 100 K using thermodynamic measurements,[3] neutron diffraction,[12] and NMR.[14,15] These measurements resulted in a previous phase diagram shown schematically in Fig. 1(a). The phase diagram exhibits dense (DS) and expanded (ES) solid phases, that is, more and less dense than the commensurate solid (CS); a 2D triple point of 56 K and a 2D critical temperature of 69 K. At coverages above one layer, the commensurate phase in the first layer disappears and melting, which is first order, proceeds from an expanded solid or low-density phase. Our data largely confirm these results but we find that the commensurate phase persists when the coverage is above one layer, and melting proceeds directly from that phase [Fig. 1(b)].

The maximum thickness of liquid or solid film that can form on the adsorbate surface depends on the relative strengths of the molecule-substrate potential and the molecule-molecule interaction. For solid films, it can also depend on the lattice mismatch between the substrate or the first layer of adsorbate and the natural lattice spacing of the bulk adsorbate. If an infinite number of layers form on the substrate, wetting is called complete. Wetting is incomplete if only a finite number of layers can form. The review by Hess enumerates the various wetting properties of adsorbates on graphite.

Wetting of methane on graphite has previously been studied using vapor-pressure isotherms on powder substrates[2,7,8] (e.g., Grafoam, Grafoil, ZYX, Papyex) and graphite fibers,[9] as well as ellipsometry,[5] and low-energy electron diffraction (LEED) and reflection high-energy electron diffraction (RHEED) on single crystals. In the isotherms on powder substrates, up to 3–4 steps can be seen corresponding to the formation of distinct layers of film. The fiber isotherms show at least 6 methane layers above 70 K, with the number of layers increasing as the temperature approaches the triple point, T_t. Ser, Larher, and Gilquin[19] have pointed out the difficulty of judging complete wetting using vapor-pressure isotherms on powder substrates as well as fibers, due to the effects of capillary condensation. Scattering experiments on xenon[20] and argon[21,22] on powder substrates show the existence of capillary condensed material coexisting with film. Our recent results[23] are consistent with these findings. On single crystals, RHEED measurements show evidence of flat films up to nearly 15 layers between 14 and 40 K. LEED shows at least four layers between 35 and 40 K. Ellipsometry studies have shown 8–10 layers for $42 < T < 76$ K.

The growth of films on the substrate can be characterized as being layer by layer or continuous.[1] Layer-by-layer growth manifests itself in an adsorption isotherm (number adsorbed versus pressure) as sharp steps. The step height is approximately equal to a molecular layer and the step represents a crossing of the coexistence region between an n-layer film and an $(n+1)$-layer film.

As the temperature is increased, this coexistence region can terminate in a critical point. A family of vapor-pressure isotherms combined with specific-heat data can be used to map out the location of the coexistence regions and the layer critical points. From vapor-pressure isotherms, Larher and Angerand[7] concluded that the layer critical points for the second, third, and fourth layers are 82.5, 82.5, and 86.7 K, respectively. Preliminary ellipsometry data by Gemmill, Wu, and Hess[24] yield layer critical points of about 79 and 85 K for the third and fourth layers, respectively. Our data confirm those results for the second layer, while our third-layer value is not inconsistent with either of the third-layer results. Our fourth-layer value critical point is lower than the previous fourth-layer values.

Neutron diffraction measurements[10] indicate that below 50 K the completed monolayer has a smaller lattice spacing than that in bulk solid methane. For coverages between 1.8 and 2.5 layers, the line shape is best fitted to a composite bilayer and monolayer line shape, which the authors interpret to mean the bilayer is composed of regions where the two layers are mutually commensurate surrounded by regions where the layers are incommensurate with each other. Above 2.5 layers, the line shape suggests that a commensurate *ABC* stacked trilayer is formed, without ever passing through a region of commensurate bilayer. Monte Carlo simulations[25] on a small (672 particles) system implied that the two layers in a bilayer would be incommensurate with each other, with the two layers rotated with respect to each other over the entire sample and that there would be an oblique unit cell. The rotation and the oblique unit cell were not seen in the diffraction measurements. Molecular-dynamics[26] simulations on bigger systems (up to 20 000 particles) predict a commensurate-incommensurate transition between the first two layers as coverage is increased. The molecular-dynamics simulations also reveal the presence of domain walls between *AB* and *AC* stacked regions and suggest that this structure explains the bilayer diffraction data.

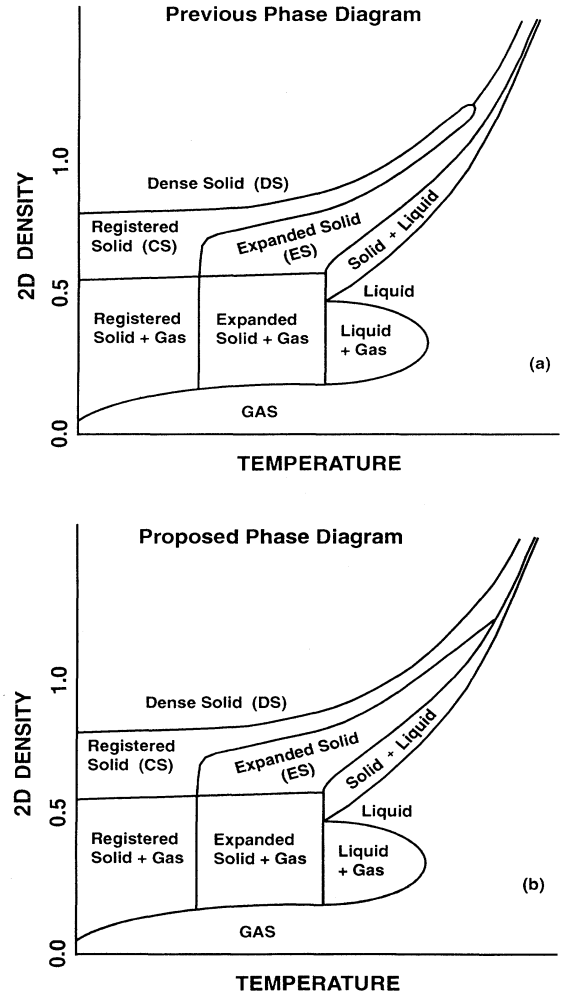

FIG. 1. (a) 2D film density vs T schematic phase diagram for methane on Grafoam proposed by Kim, Zhang, and Chan (Ref. 3). Note that the CS phase region ends at high coverages, leaving the DS-to-ES phase transition. (b) Proposed extended first-layer phase diagram, as discussed in the text. These phase diagrams are schematic only since the number in the first layer is not generally known once overlayers start to form.

Capillary condensation was expected to become the dominant form of adsorption in this system for coverages above 5 nominal layers, so we studied its effects by checking in adsorption isotherms for hysteresis. We find that hysteresis is, indeed, present at coverages beginning at 1.1 layers. However, by comparing the heat-capacity signals attributed to the film on the two branches of the hysteresis curve, we find that phase boundaries in the μ vs T plane are not significantly affected by the presence of capillary condensate. Thus it remains possible to study the phases of uniform films in spite of capillary condensation.

The principal phase boundaries are most easily seen in Fig. 2, where the positions of heat-capacity peaks are plotted in the N (number adsorbed) vs T (temperature) plane. The peaks are connected by solid curves indicating the presence of presumed phase boundaries. The two curves at ~ 100 and ~ 110 K are due, respectively, to an IC-C (incommensurate-commensurate) transition and to melting of the first layer. This is what we refer to as the extended monolayer regime, because the behavior of the monolayer is influenced by the presence of up to three layers adsorbed on top of it. The curve at ~ 90 K is due to melting of the capillary condensate that coexists with the film over the entire region shown. The structure in the region 75–85 K and 200–500 STPCC represents the gas-liquid-solid phases of the second layer and possibly an IC-C (with respect to the first layer) transition as well. Similar structures, somewhat distorted because N contains some capillary condensate, may be seen for the third and fourth layers, at slightly lower temperature. There are also a number of features that are not well understood, as we shall describe below.

Experimental details are described below in Sec. II. Because capillary condensation has been poorly understood in previous multilayer studies, we devote a separate section to discussing its effects, Sec. III. Results and dis-

cussion regarding multilayer films are presented in Sec. IV, and conclusions are in Sec. V.

II. EXPERIMENTAL DETAILS

The heat-capacity and vapor-pressure isotherm data were taken with a homemade automated scanning ratio calorimeter, sketched in Fig. 3. It is loosely based on a design implemented by Buckingham, Edwards, and Lipa[27] and is particularly useful for finding small heat-capacity features on the large Grafoam background. The sample heat capacity, C_{sample}, is found by comparing it to the heat capacity of a comparison thermal mass, C_{ctm}. Active, computer-controlled feedback is used to keep the sample and comparison thermal mass in an adiabatic environment at all times. During operation, the heat input to the comparison thermal mass, W_{ctm}, is constant, causing its temperature to rise linearly with time. The sample's heat input, W_{sample}, is varied to make its temperature closely follow that of the comparison mass. Ignoring stray heat leaks, the sample heat capacity is

$$C_{\text{sample}} = \frac{C_{\text{ctm}} W_{\text{sample}}}{C_{\text{ctm}} \delta\dot{T} + W_{\text{ctm}}} ,$$

where $\delta\dot{T}$ is the time derivative of the temperature difference, δT, between the sample and the comparison masses. The heat-capacity data are reproducible to $\pm 0.1\%$ and the noise for data points separated by 0.1 K is less than $\pm 0.04\%$ of the background (including the Grafoam and heat-capacity cell), for 2 K/h scanning rates. δT is typically below 0.05 K, even with rapid changes in the sample heat capacity. More points per degree can be obtained by operating at slower drift rates, with similar calorimetric accuracy. Heat-capacity scans were performed from 65 to 120 K over 28 h of continuous operation. The heat-capacity data that will be presented were obtained with a scanning rate always less than 2 K/h, and each point is calculated as a fit to a least-squares cubic curve for data taken over 3 min. Points are reported every 3 min so the data are statistically independent. There should be no visible smoothing in the data.

Chemical potentials are deduced from vapor-pressure measurements, made using a room-temperature 1000-torr capacitive manometer, typically linear to within 0.05% of full scale. A cyrogenic valve in the fill tube allowed the

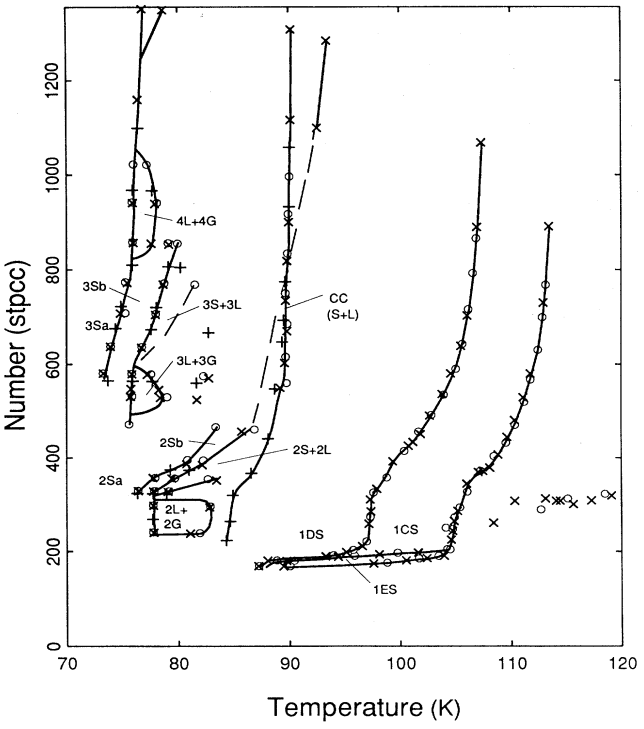

FIG. 2. Locations of the peaks in the heat capacity for films on the adsorption and desorption branches in the number adsorbed, N, vs temperature, T, plane. STPCC means cm^3 at standard temperature and pressure. X denotes the location of peaks on the adsorption branch with the cryogenic valve open and circles are for data taken with this valve closed. For the points on the desorption branch (crosses) the number adsorbed is reduced by the distance between the upper and lower boundary curves in Fig. 4. S, L, and G refer to solid, liquid, and gas. The numbers refer to the layer number. Sa and Sb represent possible solid phases, commensurate and incommensurate with the underlying layer. CC represents the capillary condensate melting region. The solid lines connect unambiguous peaks in the heat-capacity data, while the dashed lines represent conjectured peak continuations. DS, CS, and ES refer to dense, commensurate, and expanded solids, respectively. Other features are described in the text.

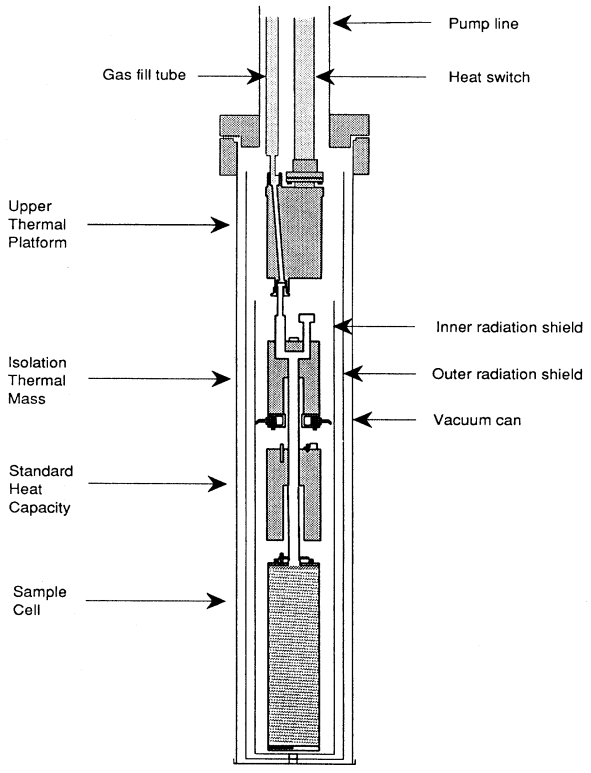

FIG. 3. Configuration of the scanning ratio calorimeter and its adiabatic surroundings.

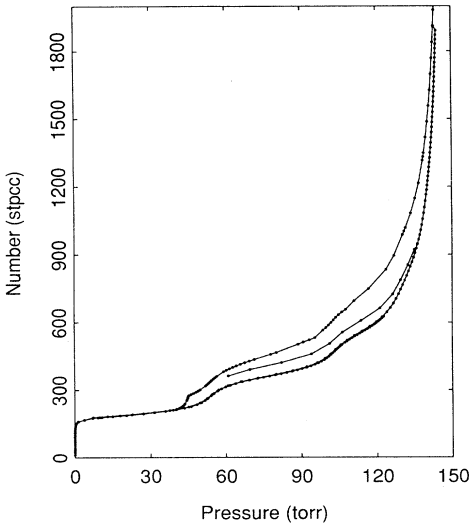

FIG. 4. Vapor-pressure isotherm N vs P taken at 95 K for the adsorption branch and two downward scanning curves, starting at 11 (upper curve) and 5.5 (central curve) layer adsorbed. N is the amount adsorbed in STPCC's.

cell's dead volume to be reduced in some experiments, at the cost of not allowing vapor-pressure measurements. Details of the apparatus and experimental procedures can be found in Refs. 28 and 29.

We used the inflection point of the first step on an adsorption isotherm to determine the monolayer capacity. Since Hamilton and Goodstein[2] made a rigorous measurement of the surface area of their sample, the surface area for this experiment was found by comparing the vapor-pressure isotherms on our larger substrate with those data. A scaling factor times Hamilton's monolayer capacity gives the monolayer capacity. We measured an isotherm at 95 K, starting at zero coverage, shown as the bottom curve in Fig. 4. The scaling factor was found to be 2.134, resulting in a monolayer coverage of 194 STPCC for our substrate. The $\sqrt{3}\times\sqrt{3}$ coverage is about 85% of this value.[30]

III. CAPILLARY CONDENSATION

Since the possibility of capillary condensation in this system had been suspected, we carried out measurements to characterize its effects. The results have been discussed in a previous paper[23] but we discuss them briefly here.

We measured a vapor-pressure isotherm at 95 K, going both upwards and downwards in coverage, in order to check for hysteresis. Inaba and Morrison[8,31] had previously reported hysteresis in vapor-pressure isotherms in the methane-Grafoam system for temperatures about 84.5 K. Meanwhile, a neutron-scattering study found capillary condensation in argon,[22] while an x-ray-scattering study of xenon films on exfoliated graphite found capillary condensate coexisting with films as thin as a monolayer on the desorption branch of their isotherm.[20]

Figure 4 shows the isotherm we obtained at 95 K. The outer curves are called boundary curves while the inner line is a scanning curve. The lower boundary curve (adsorption branch) is found by adding doses of gas to an initially empty surface, while ideally, the upper boundary curve (the desorption branch) is found by removing doses of gas from an initially saturated state. Going up or down in coverage from an intermediate coverage results in a scanning curve. The upper and lower curves join at a surprisingly low 1.1 layers, but the corresponding relative pressure, 0.27, is not unusual for capillary condensation. The boundary curve would presumably join again when the Grafoam substrate is filled at a much higher coverage. The upper curve in Fig. 4 started from a nominal coverage of 11 layers while the middle curve started at a nominal coverage of 5 layers. Since the upper curve has lower pressure at any given coverage, it is the more stable branch, while states in the adsorption branch are metastable. Since previous studies of multilayer films had no consistent procedure of film preparation, it was important to characterize the effect on the specific-heat signals of different ways of preparing the film.

In Ref. 23, we presented heat-capacity data for three films with the same nominal coverage located on the different branches in Fig. 4. The data showed that the appearance and location of specific-heat features are strongly dependent on the way the film was prepared. The adsorption branch, although technically metastable, was extremely reproducible.

Although these results seem to preclude the study of multilayer (>1.1 layers) films on exfoliated graphite, Fig. 5 shows that when peaks from both the adsorption and

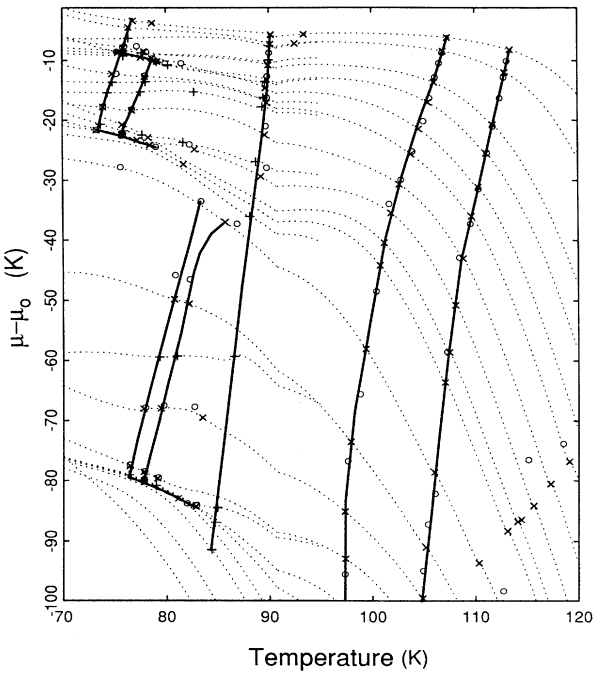

FIG. 5. Locations of the peaks in the heat capacity in the μ vs T plane for the higher coverages. Crosses are for data taken with the cryogenic valve open on the desorption branch; X, on the adsorption branch with the valve open; and circles are for data taken with this valve closed. The dashed lines represent the path traveled by the system as the film was warmed. Heavy lines connect similar peaks together to form phase boundaries.

desorption branches are plotted in the μ-T plane, the resulting phase boundaries are independent of the branch the data were taken on. The properties of the adsorbed film may be observed as a function of the chemical potential, independent of the amount of capillary condensate. In addition, if a phase diagram in the N vs T plane is corrected for the amount of capillary condensate (this amount is roughly the difference between the upper and lower branches of the isotherm), the adsorption and desorption branch data also agree with each other, as seen in Fig. 2. There is no strong interaction between the film and the capillary condensate. This is an important result regarding capillary condensation, because it means that it is still possible to study multilayer films, at least up to about 5–6 layers, but the film thickness is not given by the amount adsorbed. Accurate vapor-pressure hysteresis curves at several temperatures are needed to correct the coverage to find the thickness of the uniform film for coverages less than 2 or 3 layers. For thicker films, capillary condensation occurs on both the branches of the adsorption isotherms. Nevertheless, although the film thickness may not be known precisely, film properties may be discussed in terms of chemical potential. Beyond about 5–6 layers, most of the molecules adsorbed into the system go into the capillary condensate.

IV. RESULTS AND DISCUSSION

The heat-capacity data may be grouped into two types, those taken on the adsorption branch (from 70 to 120 K) and those on the desorption branch (70 to 95 K). All the data for films on the adsorption branch were recorded twice, first with the cryogenic valve closed, thus decreasing the dead volume of the system, but preventing the simultaneous pressure measurement, and then again with it open. All the runs on the desorption branch were made with the cryogenic valve open.

Figures 6 and 7 show the adsorption branch heat-capacity data, without the desorption correction, plotted together. There are four major features in the data: (1) The large peaks from about 100 to 112 K in Fig. 6 are attributed to the continuation of first-layer melting, while the small peaks about 8 K lower on each curve are due to the commensurate to incommensurate phase transition in the first layer at high coverages. These peaks will be used to make some modifications to the existing extended monolayer phase diagram and will be discussed in Sec. IV A. (2) The small peaks from 75 to 85 K, enlarged in Fig. 7, are related to the 2D phase diagram for the uppermost layer of the film and will be discussed in detail in Secs. IV B and IV C. (3) The peaks near 90 K have been shown to be the melting of the capillary condensate and are discussed in a separate paper.[32] (4) The broad peaks from 112 to above 120 K are likely to be due to the desorption of the film when the experimental path passes downwards through the first step in the vapor-pressure isotherm. These will be discussed in Sec. IV D.

The locations of all the peaks from both the adsorption and desorption branch data in the N_{film} vs T plane are shown in Fig. 2. The lines follow the peaks through the different coverages and represent phase boundaries. Fig-

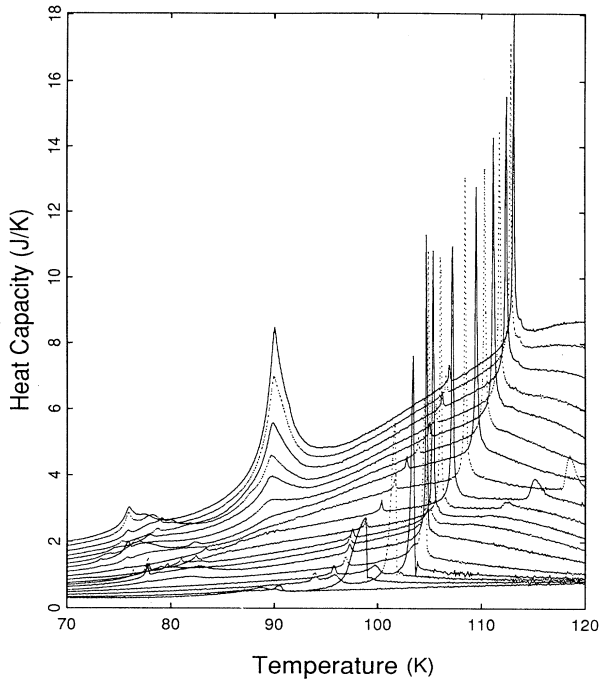

FIG. 6. Heat capacity for films on the adsorption branch with the cryogenic valve closed, uncorrected for desorption. Coverages are 0.87, 0.94, 1.03, 1.12, 1.25, 1.55, 1.70, 1.85, 2.06, 2.44, 2.67, 3.00, 3.30, 3.66, 4.00, 4.43, 4.87, and 5.27 layers in the system (gas, film, and capillary condensate).

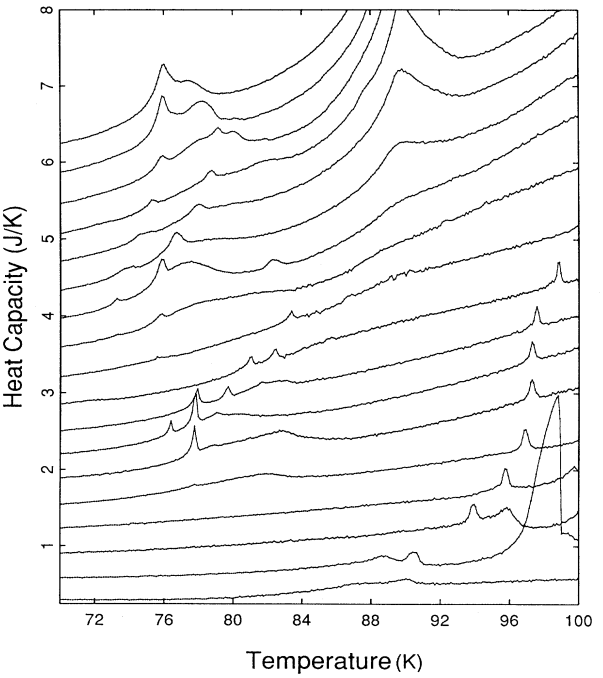

FIG. 7. Heat capacity for films on the adsorption branch with the cryogenic valve closed, uncorrected for desorption, from 70 to 100 K. Each scan was stepped upwards by 0.25 J/K, with the highest coverage run at the top of the plot. Coverages are 0.87, 0.94, 1.03, 1.12, 1.25, 1.55, 1.70, 1.85, 2.06, 2.44, 2.67, 3.00, 3.30, 3.66, 4.00, 4.43, 4.87, and 5.27 layers in the system (gas, film, and capillary condensate).

ures 5 and 8 show the $\mu-\mu_0$ vs T phase diagram, with the dashed lines representing the system's path as the temperature increased in each scan.

A. First-layer melting peaks

The heat-capacity data of Kim, Zhang, and Chan[3] (KZC) map out the monolayer phase diagram up to 1.0 layers adsorbed, from 5 to 100 K, shown in Fig. 1(a). We observe interesting features of the monolayer phase diagram, often called the "extended" monolayer regime, at temperatures up to 120 K, and overall coverages up to five layers.

The tall, sharp peaks above 100 K in Fig. 6 are continuations of the first-layer melting peaks found by KZC. They found that the monolayer melting heat-capacity peak does not disappear near monolayer completion, as concluded by early heat-capacity studies,[33,34] but continues to higher coverages and temperatures. This result is not surprising, and has since been observed[35] for other systems. An explanation for the sudden elevation of the melting temperature, T_M, near monolayer completions has been suggested by Etters, Roth, and Kuchta.[36] The authors postulate that the presence of vacancies between islands in a partial monolayer promotes thermal fluctuations in the substrate plane, which lead to self-diffusion, thermal expansion, and melting at T_M. Completed monolayers, on the other hand, are impeded from thermal expansion by the constant area of the substrate and therefore require fluctuations in the z direction to initiate melting. These fluctuations normal to the substrate plane require forces about an order of magnitude larger than lateral forces, and thus, melting of completed monolayers should occur at higher temperatures than the melting of partial monolayers.

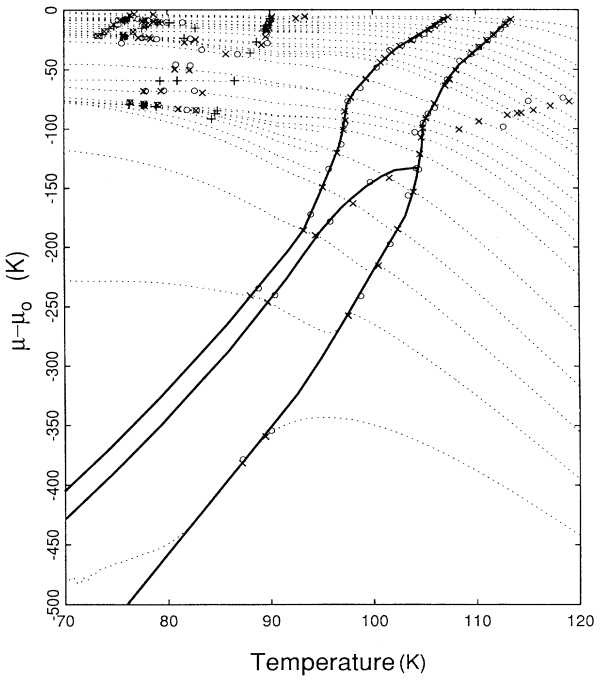

FIG. 8. Locations of the peaks in the heat capacity for films on the adsorption and desorption branches in the $\mu-\mu_0$ vs T plane for all coverages, where μ_0 is the chemical potential of bulk methane at each temperature. Crosses are for data taken with the cyrogenic valve open on the desorption branch, X denotes the location of peaks on the adsorption branch with the valve open, and circles are for data taken with this valve closed. The dashed lines represent the path traversed by the system as the film was warmed. Heavy lines trace out the incommensurate-commensurate phase transitions and the melting transition of the extended monolayer regime.

The first-layer melting peak also increases in size drastically and becomes much narrower when the monolayer completes. This can be explained by a similar argument by Elgin and Goodstein.[37] The film expands when melting at constant pressure, just as bulk materials generally do. Below monolayer completion, this effect merely causes the two-dimensional spreading pressure to rise. However, at higher coverages, the melting process overcomes the adsorption forces enough to promote some molecules to the second layer. Work is done against the adsorption forces, requiring larger heat input, and reducing the first-layer density, which in turn lowers the melting temperature. These effects combine to increase the apparent height and reduce the width of the heat-capacity peaks.

There are small peaks in our data about 7–8 K below the melting peaks in Fig. 6. These peaks can be associated with commensurate-incommensurate transitions prior to melting. Vora, Sinha, and Crawford[12] identified all the phases and the approximate locations of the phase boundaries of monolayer methane using neutron diffraction. They identified six two-dimensional phases: dense incommensurate solid (DS), commensurate solid (CS), and expanded incommensurate solid (ES), supercritical fluid, gas, and liquid. They proposed a phase diagram in which the CS phase ceases to exist at high coverage and temperature and postulated that there was a phase transition from DS to CS phase at about 0.88 layers. KZC described the shape of the boundaries between these phases and continued the CS phase region upwards to higher temperatures and coverages. They still ended the CS phase region, implying that there is a phase transition between the two incommensurate phases, ES and DS, as shown in Fig. 1(a).

From our data at much higher coverages and temperatures, it is clear that the first-layer phase diagram needs further modification. Figure 9 displays the small features in the heat capacity just below first-layer melting from 0.87 to 1.33 monolayers coverage. In the two lowest coverage scans, the features are very broad and hard to see at the scale shown. The small bump in each of these runs is on the first-layer melting curve shown in Fig. 8, so they can be identified as due to first-layer melting. The DS to CS and the CS to ES phase transition heat-capacity peaks are below 65 K and are not seen. Three phase transitions, DS to CS (I), CS to ES (II), and ES to liquid (III), are clearly visible in the runs from 0.930 up to and including 1.140 monolayers, shown in Fig. 9. The temperature difference between features I and III is approximately constant for all the plots above 0.930 monolayers, but

peak II moves from just above I to just below III in the coverage range from 0.930 to 1.140 monolayers. At 1.334 monolayers, peak II is consumed by III. Since the phase boundary between the ES and CS phases (peak II) ends on the first-layer melting line, the expanded solid region of the phase diagram ends between 1.140 and 1.334 monolayers. The location of these points in the $\mu-\mu_0$ phase is shown in Fig. 8. At high coverages, as the temperature is raised, the monolayer changes from the DS to CS phase, then the CS phase melts. This new phase diagram is shown in Fig. 1(b). We find this diagram more satisfying than Fig. 1(a) because the phase boundary in Fig. 1(a) between DS and ES would represent a phase transition between two phase of the same symmetry and the same density. No such phase transition should occur. (The DS and ES phases would meet at the same density, even though they are defined to be more dense and less dense, respectively, than the CS phase because, in the region of the phase diagram described, the CS region no longer exists.)

In Fig. 2, there is a steep section followed by a sudden jog in the slope of the first layer's DS-CS transition and melting lines in the region with 200–400 STPCC adsorbed, that is not present in Fig. 1(b). The near vertical part is also mimicked in the CC (capillary condensate) melting line. During the formation of the second layer, the chemical potential, μ, changes by very little, so the states coexisting with the second layer, i.e., the first layer and the capillary condensate, would not change very much with temperature. This would account for the steepness. We believe that the sudden jog is due to second-layer completion, so that it shows up in a plot of the total amount adsorbed (Fig. 2) but not a plot of the amount adsorbed in the first layer (Fig. 1). At the completion of the second layer, the first layer is compressed, thereby increasing its melting temperature.

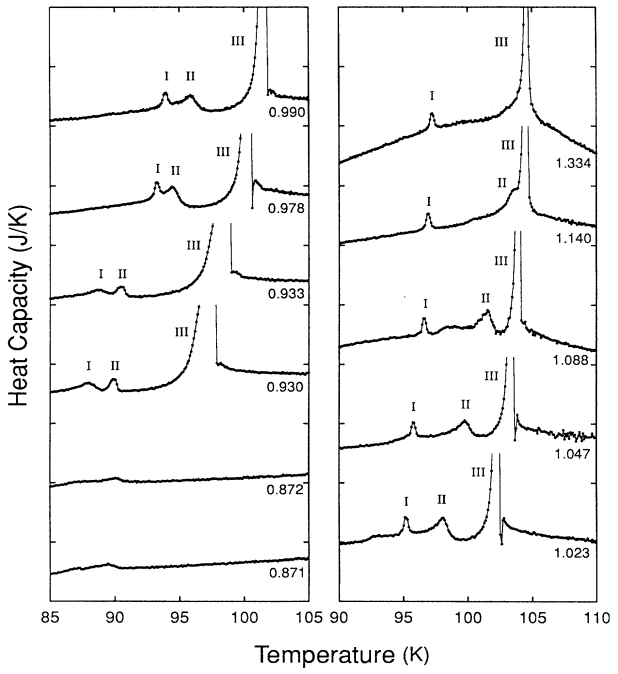

FIG. 9. Heat-capacity peaks associated with the extended monolayer region. The number of monolayers in the film at the point of the DS-to-CS phase transition (lowest temperature feature) is indicated below each curve. I, II, and III refer to the DS-to-CS, CS-to-ES, and ES-to-liquid transitions, respectively.

Figure 7 shows heat-capacity peaks that locate at least seven distinct phase boundaries in the second, third, and fourth layer. In general, the phase diagram of each of these layers is similar to the first-layer phase diagram, and includes a 2D liquid-gas coexistence region (as described by Ref. 2), and a 2D triple point. Because the individual layers in a multilayer film interact with each other, it is not strictly correct to identify a phase boundary with a phase transition in any particular layer. But these phase transitions often occur only in a single layer, so it is convenient to associate the features with a layer in the film.

Hamilton and Goodstein[2] (HG) reported a series of bumps in the heat capacity at temperatures between 75 and 80 K. These bumps were attributed to layer-by-layer condensation. Six blunt-nosed 2D liquid-gas coexistence regions were proposed, and the heat-capacity peaks were thought to represent the experimental path passing out of these coexistence regions. In the limit of infinite film thickness, these phase transitions were expected to become the bulk roughening transition. This basic conclusion may stand, but, as may be seen in Fig. 7, the much higher resolution of the present measurement shows that the bumps reported by HG masked a much more complex set of features that we now discuss.

The coverages mentioned in the discussion below are either the coverages on the adsorption branch, where there is less capillary condensation, or (for the desorption branch) the number adsorbed less the vertical distance between the branches on the vapor-pressure isotherm. Therefore all the coverages are relative to the total amount adsorbed on the adsorption branch, but not to the uniform film thickness, because there is a significant amount capillary condensed above three layers adsorbed even on the adsorption branch. Unfortunately, we have no accurate way to measure the amount capillary condensed on the adsorption branch. Perhaps other experimental techniques (x-ray or neutron scattering) may be used to find this quantity in the future.

B. Second-layer phase diagram

Figure 10 shows the heat-capacity signals associated with the second uniform layer. The scans are displayed with the lowest coverage at the bottom of the plot, so the topology of the N vs T phase diagram can be made by connecting the similar phase transitions to form the phase boundaries. The result, shown in the inset, can be identified as a feature in Fig. 2. Since, in the temperature range shown, the number in the first layer is relatively constant during second-layer formation, the N vs T phase diagram is similar to the 2D density versus temperature phase diagram for the second layer. However, Fig. 2 shows that the melting temperature of the first layer continues to increase in the coverage range from about 200 to 500 STPCC. When the first layer is covered by the

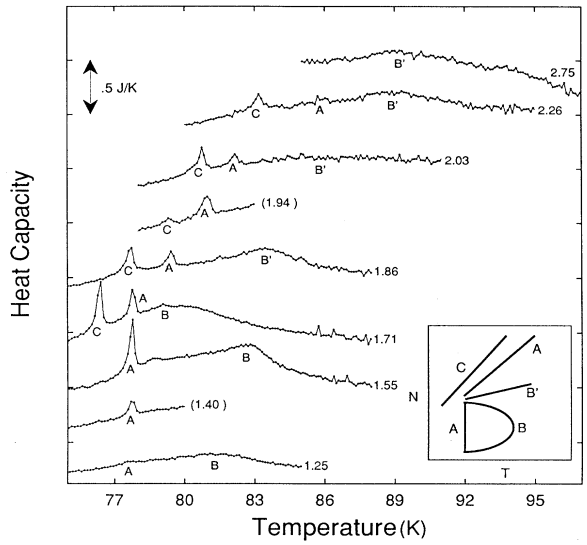

FIG. 10. Heat-capacity signals identified with the second layer. Numbers indicate the total amount (layers) in the system during the scan. Numbers enclosed in parentheses indicate desorption branch data whose coverage is reduced by the additional amount capillary condensed on that branch, relative to the adsorption branch. Letters identify heat-capacity features for discussion in the text. The inset corresponds to the feature at about 75–80 K and 200–500 STPCC in Fig. 2.

second (or more layers), the first-layer melting temperature is a function of the first-layer density, and a function of the energy necessary to promote a molecule into the other layers. Therefore the first-layer density is increasing slightly in this coverage range. The first-layer density can change the phase diagram of the second layer because the first layer is the "substrate" for the second layer.

The second-layer heat-capacity peaks in Fig. 10 are labeled $A-C$. Heat-capacity peak A is clearly identified as the second-layer melting peak. In the four heat-capacity runs, at 1.25, 1.40, 1.55, and 1.71 layers, this sharp peak rapidly increases in size, but appears at exactly the same temperature, 77.7 K, the 2D triple point for the second layer. This peak should increase in size at the same temperature as the coverage increases, until the 2D condensed phase completes. Then there will be no more 2D vapor phase and the melting peak should move to higher temperature. If there is a triple point, there should also be a liquid-vapor coexistence region and associated heat-capacity features, labeled B in Fig. 10. The location of B traces out a blunt-nosed phase boundary that seems to join with the melting peak near 1.71 layers. This interpretation is confirmed in Fig. 5, where it is seen that the locations of the B peaks collapse into a single line in the μ-T plane, as they should for a coexistence region. The locations of the B features suggest a second-layer critical point of about 83 K, which is consistent with the results of Larher and Angerand[7] from vapor-pressure isotherms. At 1.71 layers another phase transition also appears, peak C, below peak A in temperature. At higher coverages, peaks A and C move to higher temperatures at the same distance apart, about 2 K. Contrary to our expectation, at higher coverages (1.86), another feature (B') appears that is similar in shape to B, and at a temperature higher than peak A. At yet higher coverages, peaks A, B', and C move together to higher temperature while peak B' broadens. Then A and C seem to disappear suddenly at about 2.75 layers. Above this coverage, B' seems to disappear or become too low and broad to identify.

Examining the termination of B' on Fig. 7 shows that the capillary condensate triple point peaks on the adsorption branch begin near where feature B' disappears. On the desorption branch, the triple point peak is very large and also near where B' terminates. Thus B' may be the first bit of capillary condensate melting. On the other hand, if B' is a feature of the film, it is unlikely that it ends on the capillary condensate melting curve, since the two systems (capillary condensate and uniform film) do not interact significantly. If B' is not due to capillary condensation, it could be due to a structural phase transition in the first layer whose occurrence is made possible by the less rigid structure of the now liquid upper layer. Monte Carlo simulations by Phillips[38] suggest the promotion of atoms to the next upper layer as vacancies are created in this layer. Eventually, this results in the disordering and subsequent melting of this lower layer.

There have been two neutron scattering studies of multilayer methane on graphite done at the Brookhaven National Laboratory. All the data in the first study[10] were taken at low temperature, ($T \leq 50$ K). They found that the monolayer lattice spacing is about 1% smaller than the bulk (i.e., the monolayer is more dense than the bulk). As the film is made thicker, the signal from a bilayer film that has the second-layer incommensurate with the first appears. Thicker films have a trilayer structure (all the layers mutually commensurate) with nearly the bulk density. The results for thicker films are, unfortunately, questionable because the bulk signal was masked by the signal from the graphite, and therefore no bulk capillary condensate was observed (as noted by Morishige *et al.*[20]).

In a second study, Larese and Zhang[39] have recorded neutron scattering data at higher temperatures for methane on graphite and their data indicate a possible registry transition in the second layer. They state that the second layer is incommensurate with the first at low coverages, but as the coverage is increased there is a phase transition to a denser phase that has the second layer commensurate with the first. Feature C may be the heat-capacity signal from this phase transition. At low temperature and high coverage, the layers are commensurate and as the temperature is raised, the second layer becomes incommensurate with the first. This would explain why this phase transition appears near layer completion, where the 2D vapor disappears. On the other hand, because the incommensurate-commensurate phase transition discovered by the neutron scattering study was supposed to have a nearly horizontal phase boundary in the N vs T plane, it may be invisible in the heat-capacity data. Then feature C would be caused by a different (unknown) phase transition.

There are several possible explanations for the disappearance of the A and C peaks at the highest coverage in

Fig. 10. A phase boundary may suddenly curve towards the horizontal in the N vs T plane and thus become invisible because the experimental path no longer crosses it. Alternatively, a phase boundary could end in a higher-order phase transition that would be hard to detect with calorimetry.

In the first case, the peaks could reappear at a higher temperature at higher coverages, or end on another phase boundary (first-layer melting, perhaps). This possibility is supported by the known example that the melting peak for the first layer of methane jumps upward 30° in temperature just above layer completion. While it is increasing, the first-layer melting peak becomes difficult to detect with calorimetry, and was originally missed by several experimenters.[33] The location of the capillary condensate triple point peaks at higher coverage could mask peaks A and C. Small peaks do appear just above the temperature of the capillary condensate melting peaks at 6.0 and 7.0 nominal layers adsorbed (not shown, but plotted in Fig. 2). These are possibly the continuation of A, second-layer melting.

C. Third- and fourth-layer phase diagrams

The third-layer N vs T phase diagram is again similar to the standard liquid-solid-vapor density versus temperature phase diagram. Figure 11 shows the heat-capacity scans for the coverages with peaks (labeled $D-G'$) likely to be related to the third layer. The locations of these peaks are also shown in the N vs T phase diagram, Fig. 2. Note that both adsorption and desorption data are shown, with only very small differences between them. Peak D appears at nearly constant temperature while the coverage is increased and therefore can be identified as

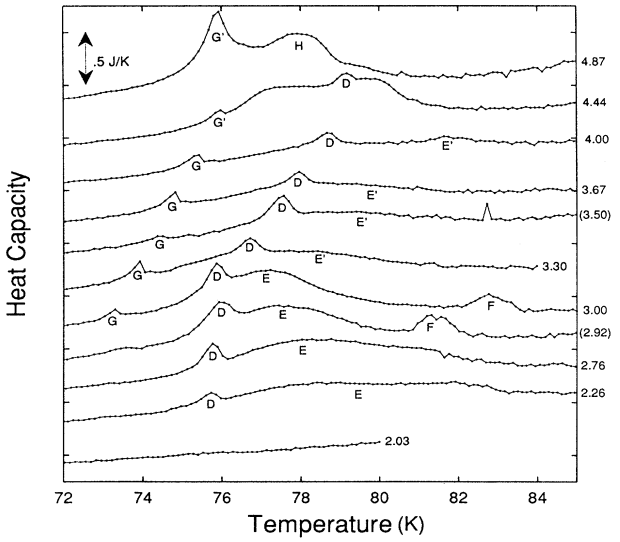

FIG. 11. Heat-capacity signals possibly identified with the third layer. Numbers indicate the total amount (layers) in the system during the scan. Numbers enclosed in parentheses indicate desorption branch data whose coverage is reduced by the additional amount capillary condensed on that branch, relative to the adsorption branch. Letters identify heat-capacity features for discussion in the text.

the signal from the third-layer triple point. Following peak D is a broad feature, E, that traces out the liquid-gas coexistence region. This interpretation is once again confirmed in the μ-T plane in Fig. 5, where the positions of the E features collapse along a single line, to within the experimental error, supporting the existence of a coexistence region, with a layer critical temperature of about 80 K. As with the second layer, however, there are surprises.

Peak F is far larger than the noise in the data, and is reproduced in three data runs at coverages between 2.9 and 3.0 layers. Two of the data runs are on the adsorption branch, taken from the same film (only one of these is shown), but the other was from a desorption branch film from a different cell filling. The peak appears at a similar position in the N vs T plane for the data from both branches, adsorption and desorption. However, this feature cannot be seen to connect with any phase boundary at either higher or lower coverages. The reasons why a phase boundary could become invisible to the heat-capacity data have been outlined above. But in this case, the feature is unconnected to any boundary, existing only over a short range of coverages. We have no explanation for this behavior. However, it is interesting to note that these features are located close to Larher and Angerand's third-layer critical temperature.[7]

Just as in the second layer, another peak appears in the third layer, G, a few degrees below the 2D triple point peak (D), on the highest coverage run before the closure of the liquid-gas coexistence region. For higher coverages, the peak D moves to higher temperatures, just as melting does in the standard liquid-solid-vapor phase diagram. Also like the second layer, there is still a remnant, feature E', of E at coverages above the closure of the liquid-gas coexistence region, but E' is so small, it may not be real. If it is real, it could be due to a similar event in the second layer driven by the melting of the third layer, as postulated for peak B' earlier. Peaks D and G move to higher temperature as the coverage is increased until features appear that mark the appearance of the fourth layer. Unlike the second layer, where peaks A, B', and C disappear at a temperature far above any peaks in the third layer, the third-layer peaks seem to intertwine with the fourth-layer peaks. In particular, third-layer peak G seems to merge into fourth-layer peak G' at 76 K.

Peak G' can be identified as the fourth-layer triple point peak in Fig. 12. At the coverage where peak G appears, 3.00 layers, the fourth layer is only beginning to be populated with 2D gas. There should be no fourth-layer solid at this coverage, and peak G is very similar to peak C in the second layer. While it is comforting to find that peak G does not just disappear, like peaks A and C in the second layer, it is surprising that it may join with what appears to be melting in the next (fourth) layer. It is possible that peak G may be the signal from an incommensurate-commensurate solid phase transition in the third layer that drives the melting of the fourth layer.

Likewise, what is presumed to be the third-layer melting peak, D, in the extended third-layer phase diagram, appears to end very close to the fourth-layer coexistence region. This behavior may be seen in the upper two

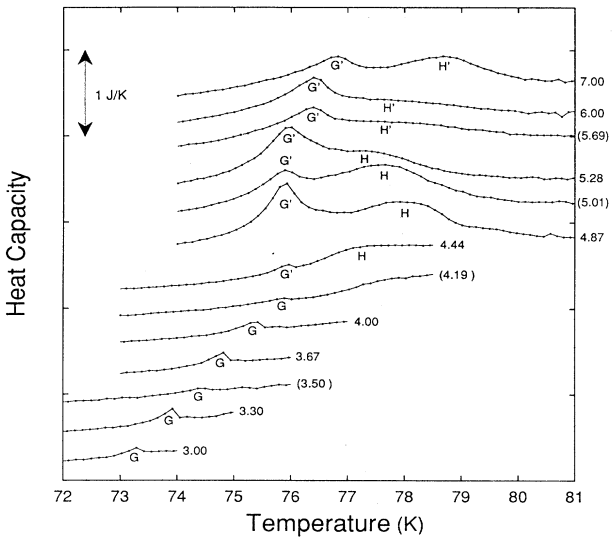

FIG. 12. Heat-capacity signals possibly identified with the fourth layer. Numbers indicate the total amount (layers) in the system during the scan. Numbers enclosed in parentheses indicate desorption branch data whose coverage is reduced by the additional amount capillary condensed on that branch, relative to the adsorption branch. Letters identify heat-capacity features for discussion in the text.

curves of Fig. 11. The heat-capacity data, with the cryogenic valve both open and closed at 4.44 layers adsorbed on the absorption branch, show three maxima in the fourth-layer liquid-gas coexistence region. In the runs at the next higher coverage, 4.87 layers, only a single peak appears. Could the melting of the third layer interact with the fourth layer?

In Fig. 12, feature H appears, by analogy with features B and E above, to map out a fourth-layer liquid-vapor coexistence region, with a critical point near 78 K. As with B and E, this coexistence region seems to be confirmed in Fig. 5 also. Between 5.28 and 5.69 nominal layers, the fourth-layer 2D melting G' increases in temperature and the signal from passing through the liquid-vapor coexistence region disappears. In the highest coverage run, however, a bump similar to H appears, H'. This bump is like E' in the third layer or B' in the second layer. Just like E' and B', it could be due to the layer underneath. But there is no sign of features at lower temperature than the melting curve in the fourth layer like those seen in the second and third layers. The second feature, C, is conjectured to be a C-IC transition in the preceding section. If this conjecture is correct, and if G is also another IC-C transition, the absence of similar peaks in the fourth layer seems consistent with the neutron diffraction report[10] of a commensurate ABC stacked trilayer, with bulk lattice spacing, low temperatures.

There seems to be a remarkable similarity between the second-, third-, and fourth-layer phase diagrams. Each has a well-defined liquid-gas coexistence region. The second, fourth, and possibly third layers have a heat-capacity feature (B',E', and H') at higher temperatures than the melting peaks (A, D, and G) at coverages above that where the 2D liquid-vapor coexistence regions end (1.86, 3.30, 5.69 layers). The second and third layers have a series of peaks that appear at coverages just above layer completion, at a lower temperature than the 2D melting curve (C and G). It is hoped that more structural studies combined with theoretical and computational simulations will be carried out to explain some of the underlying physics causing these phenomena.

The possible interconnections between the third- and fourth-layer phase boundaries recall the statement made early in this work, that it is not strictly proper to consider the layers as noninteracting. It would be expected that the properties of the underlayers would strongly affect the phases of the upper layers. It could be argued that solid layers are unlikely to form on top of a liquid one, and that a layer is not likely to be more dense than the layers below it. For thick films, it is expected that the individual layers' phase diagrams should be so interconnected that the film should be thought of as a single system, not a collection of layers. Methane films that are 4 or less layers thick may be near the transition between these two types of behavior.

The 2D triple points and layering critical points for the second, third, and fourth layers of methane are listed in Table I. Recent vapor-pressure measurements on Grafoam by Larher and Angerand yield the layering critical temperatures, $T_c(n)$, for methane and other gases.[7] Gemmill, Wu, and Hess[24] also report preliminary elllipsometry data for the layer critical temperatures. The values of $T_c(n)$ found in the present work by the location of the heat-capacity peaks that mark out the coexistence region are very similar for the second layer. The uncertainty in the location of the peaks for the third layer keeps us from claiming a clear-cut difference for the third-layer critical point from Larher and Angerand's result, although the evidence from Fig. 5 suggests it is lower than what they find. In addition, our third-layer critical point is not inconsistent with the ellipsometry results, which found a value of about 79 K. Our result for the fourth layer is different from the other experiments. Larher and Angerand obtain a fourth-layer critical point of 86.7 K, while Gemmill, Wu, and Hess give a value of 85 K. Our specific-heat data suggest a value of about 78

TABLE I. Layering critical point and 2D triple point temperatures (in K).

Layer	1	2	3	4	5
2D triple point	56 (Ref. 3)	77.7	75.9	76.0	
Layering critical points (this work)	69 (Ref. 3)	83	80±2	≥78	
Layering critical points from Ref. 7		82.5	82.5	86.7	87.5
Layering critical points from Ref. 24			79	85	84

K from the location of the H peaks. However, since the melting of capillary condensate can mask peaks above 84 K at these coverages, we cannot rule out the possibility that the H peaks are due to something else (maybe the continuation of the third-layer features) and that the fourth-layer critical temperature is higher than 78 K. The difficulties in determining critical temperatures from specific-heat and vapor-pressure isotherm data are well known.[7,40]

The value of the layering critical point for the thicker films is of particular interest because it may be close to the bulk roughening temperature for the analogous crystal face of the bulk solid. The inconsistent results at the higher coverages point out the need for more study.

D. Heat-capacity peaks above 110 K

In the heat-capacity data that are not corrected for desorption (Fig. 6) there is a prominent set of peaks beginning a few degrees above first-layer melting and extending to above 120 K. When the desorption correction is calculated using the approximation

$$\left[\frac{\partial\mu}{\partial T}\right]_N \approx \frac{d\mu_0}{dT}$$

and subtracted from the data, the peaks are eliminated to within the scatter in the data.

The desorption correction corrects for the energy required to expel the methane molecules from the film against the van der Walls force. The molecules leave the film to increase the vapor pressure of the 3D gas as the temperature of the film increases. The total heat capacity of the calorimeter with a film is equal to

$$C_{\rm tot} = C_{\rm cell} + C_N + C_{V_g} - q_d \left[\frac{dN}{dT}\right]_X ,$$

where $C_{\rm cell}$ is the bare sample cell heat capacity, N refers to the number of molecules in the film, C_N is the heat capacity of the film at constant N, C_{V_g} is the heat capacity of the gas in the sample cell at constant volume, and X represents the experimental path, $N(P(T(\text{time})),T(\text{time}))$ traveled by the system as it is warmed.[30,41,42] The total number of molecules in the gas plus film are constant. Note that this equation defines q_d implicitly. If the pressure is measured during the heat-capacity run and the cell background heat capacity is known, all the quantities can easily be calculated to find C_N except for q_d. The desorption correction, q_d, is found by a complicated thermodynamic analysis to be equal to[30,41,42]

$$q_d = \frac{3}{2}k_b T + T\left[\frac{\partial\mu}{\partial T}\right]_N - \mu - 2PT\frac{dB}{dT} + e_{\rm rot}(T) .$$

The chemical potential of the system, μ, is known from the pressure and temperature of the 3D gas. B is the second virial correction. The rotational energy per molecule (in J), $e_{\rm rot}(T)$, can be calculated as described by Hamilton.[30] $[\partial\mu/\partial T]_N$ is found by using the Frenkel-Halsey-Hill approximation,[43] $\mu-\mu_0 \propto d^{-3}$, where d is the film thickness, leading to

$$\left[\frac{\partial(\mu-\mu_0)}{\partial T}\right]_N = 0 .$$

The value of $[\partial N/\partial T]_X$ can be obtained from

$$\left[\frac{dP}{dT}\right]_X = \left[\frac{\partial P}{\partial T}\right]_N + \left[\frac{\partial P}{\partial N}\right]_T \left[\frac{dN}{dT}\right]_X .$$

Closely spaced isotherms (0.1 K apart) are required to give $[\partial P/\partial N]_T$. Because of the considerable time required to obtain these isotherms, we did not attempt to measure them. By using, instead, the 95-K isotherm in Fig. 4, we found that the correction from 90–140 K showed narrow bumps similar in location to the heat-capacity bumps at these coverages, and which were correlated with variations in the isotherm slope.

This analysis suggests that there is no phase transition in the film where the heat-capacity features above 110 K occur. However, since it is practically impossible to calculate the desorption correction at these temperatures exactly, this conclusion is not certain.

V. CONCLUSIONS

The initial purpose of this work was to examine the way 2D systems approached bulk behavior. The bulk properties of interest including the melting transition and surface roughening. Unfortunately, capillary condensation prevents us from making films much more than 5 layers thick. In addition, the heat-capacity signal from the melting of the capillary condensate may obscure any signal due to melting of the film as it approaches bulk melting behavior. The connection between 2D and 3D melting is difficult to make from this work, since the individual layer melting signals from the second and third layers seem to tie into phase boundaries related to the 2D nature of the films, or to drop off into nowhere. Presumably, thicker films might be formed on single-crystal substrates, at least to 10 layers or so,[1] in which bulk melting would have to appear.

Other heat-capacity studies have found multilayer phase diagrams with some similar features for various gases adsorbed on graphite, but none have seen the 2D layering coexistence region along with the 2D triple points and melting peaks extending to higher coverages in each layer we have presented here. Some studies have seen pieces of the second- or higher-layer phase diagrams. In ethylene, heat-capacity peaks due to layering but not due to melting for the second, third, fourth, and fifth layers have been observed.[44] In carbon monoxide, second-layer peaks that map out the layering coexistence region and the 2D triple point were observed but the melting was either not seen or not examined at higher coverages.[45] In argon and neon, melting peaks have been traced out to higher coverages, but the earlier studies did not have sufficient resolution to detect the coexistence regions and triple points.[46] Peaks similar to those reported by HG for methane were seen for the second, third, and fourth layers of argon and neon,[46,47] while a neutron diffraction experiment gave evidence of layer-by-layer melting below the triple point.[48] We have recently com-

pleted a study of argon[49] and krypton,[50] yielding a multilayer phase diagram radically different from the one presented here for methane. The data we are presenting in these studies are the first observation of complicated extended-layer phase diagrams for thicker films that we are aware of. These studies have revealed the signals of previously unknown phase transitions between the phases in each layer because the apparatus was more sensitive to small heat-capacity features than any previous instrument and because we now understand how to account for capillary condensation. Future studies of other adsorbates on graphite are in progress. It is hoped that other experimental techniques will help untangle the structure of multilayer adsorbed films.

ACKNOWLEDGMENTS

The authors would like to acknowledge many useful conversations with Professor P. Weichman, Professor M. Cross, Professor J. M. Phillips, Professor G. B. Hess, and Professor J. Larese. M.A.L. acknowledges support from the Continental Oil Fund. This work was supported by DOE Grant No. DE-FG03-85ER45192.

*Present address: Jet Propulsion Laboratory, 4800 Oak Grove Drive, Pasadena, CA 91109.

[1]G. B. Hess, in *Phase Transitions in Surface Films 2,* edited by H. Taub, G. Torzo, H. J. Lauter, and S. C. Fain, Jr. (Plenum, New York, 1991).
[2]J. J. Hamilton and D. L. Goodstein, Phys. Rev. B **28**, 3838 (1983).
[3]H. K. Kim, Q. M. Zhang, and M. H. W. Chan, Phys. Rev. B **34**, 4699 (1986).
[4]M. J. Lysek, M. S. Pettersen, and D. L. Goodstein, Phys. Lett. A **115**, 340 (1986).
[5]H. S. Nham and G. B. Hess, Langmuir **5**, 575 (1989).
[6]A. Thomy and X. Duval, J. Chim. Phys. **66**, 1960 (1969); **67**, 286 (1970); **67**, 1101 (1970).
[7]Y. Larher and F. Angerand, Europhys. Lett. **7**, 447 (1988).
[8]A. Inaba and J. A. Morrison, Chem. Phys. Lett. **124**, 361 (1986).
[9]G. Zimmerli and M. H. W. Chan, Phys. Rev. B **45**, 9347 (1992).
[10]J. Z. Larese, M. Harada, L. Passell, J. Krim, and S. Satija, Phys. Rev. B **37**, 4735 (1988).
[11]M. Bienfait, P. Zeppenfeld, J. M. Gay, and J. P. Palmari, Surf. Sci. **226**, 327 (1990).
[12]P. Vora, S. K. Sinha, and R. K. Crawford, Phys. Rev. Lett. **43**, 704 (1979).
[13]J. Krim, J. M. Gay, J. Suzanne, and E. Lerner, J. Phys. (Paris) **47**, 1757 (1986).
[14]J. H. Quateman and M. Bretz, Phys. Rev. Lett. **49**, 1503 (1982).
[15]J. H. Quateman and M. Bretz, Phys. Rev. B **29**, 1159 (1984).
[16]M. S. Pettersen and D. L. Goodstein, Surf. Sci. **209**, 455 (1989).
[17]M. S. Pettersen, M. J. Lysek, and D. L. Goodstein, Phys. Rev. B **40**, 4938 (1989).
[18]D. L. Goodstein, M. A. LaMadrid, and M. J. Lysek, in *Phase Transitions in Surface Films 2* (Ref. 1).
[19]F. Ser, Y. Larher, and B. Gilquin, Mol. Phys. **67**, 1077 (1989).
[20]K. Morishige, K. Kawamura, M. Yamamoto, and I. Ohfuji, Langmuir **6**, 1417 (1990).
[21]J. Z. Larese, Q. M. Zhang, L. Passell, J. M. Hastings, J. R. Dennison, and H. Taub, Phys. Rev. B **40**, 4271 (1989).
[22]J. M. Gay, J. Suzanne, J. G. Dash, and H. J. Lauter, J. Phys. I (France) **1**, 1279 (1991).
[23]M. J. Lysek, M. A. LaMadrid, P. Day, and D. L. Goodstein, Langmuir **8**, 898 (1992).
[24]C. Gemmill, H. Wu, and G. B. Hess, Bull. Am. Phys. Soc. **37**, 545 (1992).
[25]J. M. Phillips and T. R. Story, Phys. Rev. B **42**, 6944 (1990).
[26]J. M. Phillips and N. Shrimpton, Phys. Rev. B **45**, 3730 (1992).
[27]M. J. Buckingham, C. Edwards, and J. A. Lipa, Rev. Sci. Instrum. **44**, 1167 (1973).
[28]M. J. Lysek, Ph.D. thesis, California Institute of Technology, Pasadena, CA, 1992.
[29]M. J. Lysek, P. Day, M. A. LaMadrid, and D. L. Goodstein, Rev. Sci. Instrum. **63**, 5750 (1992).
[30]J. J. Hamilton, Ph.D. thesis, California Institute of Technology, Pasadena, CA, 1983.
[31]A. Inaba, Y. Koga, and J. A. Morrison, J. Chem. Soc. Faraday Trans. II **82**, 1635 (1986).
[32]M. J. Lysek, M. A. LaMadrid, P. Day, and D. L. Goodstein, Langmuir (to be published).
[33]R. Marx, Phys. Rep. **125**, 1 (1985).
[34]R. Marx and E. F. Wassermann, Solid State Commun. **40**, 959 (1981).
[35]A. J. Jin, M. R. Bjurstrom, and M. H. W. Chan, Phys. Rev. Lett. **62**, 1372 (1989).
[36]R. D. Etters, M. W. Roth, and B. Kuchta, Phys. Rev. Lett. **65**, 3140 (1990).
[37]R. L. Elgin and D. L. Goodstein, in *Monolayer and Submonolayer Helium Films,* edited by J. G. Daunt and E. Lerner (Plenum, New York, 1973).
[38]J. M. Phillips, Phys. Lett. A **147**, 54 (1990).
[39]J. Z. Larese and Q. M. Zhang (private communication).
[40]See, for example, discussion in J. Chem. Soc. Faraday Trans. II **82**, 1817 (1986).
[41]J. G. Dash, *Films on Solid Surfaces* (Academic, New York, 1975).
[42]R. L. Elgin, Ph.D. thesis, California Institute of Technology, Pasadena, CA, 1973.
[43]W. A. Steele, *The Interaction of Gases with Solid Surfaces* (Pergamon, Oxford, 1974).
[44]H. K. Kim, Y. P. Feng, Q. M. Zhang, and M. H. W. Chan, Phys. Rev. B **37**, 3511 (1988).
[45]Y. P. Feng and M. H. W. Chan, Phys. Rev. Lett. **62**, 2148 (1990).
[46]D. M. Zhu and J. G. Dash, Phys. Rev. Lett. **57**, 2959 (1986).
[47]D. M. Zhu, Ph.D. thesis, University of Washington, Seattle, WA, 1988.
[48]J. Z. Larese and Q. M. Zhang, Phys. Rev. Lett. **64**, 922 (1990).
[49]P. Day, M. J. Lysek, M. A. LaMadrid, and D. L. Goodstein, Phys. Rev. B (to be published).
[50]P. Day, M. A. LaMadrid, M. J. Lysek, and D. L. Goodstein, Phys. Rev. B **47**, 7501 (1993).